Journal of Radiological Science and Technology, 44(4), 315-325 ISSN 2384-1168(On-line) ISSN 2288-3509(Print)

<원저>

The Study of Lipid Proton Composition Change in a Rat Model of High Fat Diet Induced Fatty Liver by Magnetic Resonance Spectroscopy Analysis

Kim Sang-Hyeok·Yu Seung-Man

Department of Radiological Science, Jeonju University

고지방식이 유도성 지방간 쥐 모델에서 간의 자기공명분광 분석을 이용한 지질 양성자 조성 변화 연구

김상혁·유승만

전주대학교 방사선학과

Abstract The purpose of this study is to investigate the changes in lipid proton (LP) composition according to the induced obese fatty liver and to use it as basic data for treatment and diagnosis of fatty liver in the future. The phantom study was conducted to identify differences between STEAM and PRESS Pulse sequences in LP concentration. A high-fat diet (60%) was administered to eight Sprague-Dawley rats to induce obesity and fatty liver disease. Baseline magnetic resonance imaging /spectroscopy data were obtained prior to the introduction of high-fat diet, and data acquisition experiments were performed after eight weeks using procedures identical to those used for baseline studies. The six lipid proton metabolites were calculated using LCModel software. The correlation between the fat percentage and each LP, revealed that the methylene protons at 1.3 ppm showed the highest positive correlation. The α-methylene protons to carboxyl and diallylic protons showed negative correlation with fat percentage. The methylene proton showed the highest increase in the LP; however, it constituted only 71.86% of the total LP concentration. The methylene proton plays a leading role in fat accumulation in liver parenchyma.

Key Words: Fatty Acid, Fatty Liver, Magnetic Resonance Spectroscopy, Magnetic Resonace Imaging, Lipid Proton

중심 단어: 지방산, 지방간, 자기공명분광, 자기공명영상, 지질 양성자

Ⅰ. Introduction

Obesity and fatty liver disease is a global health challenge. In the absence of appropriate management, it can progress to chronic liver disease, such as liver fibrosis or cirrhosis [1-4]. In particular, transplantation of more than moderate fatty liver in patients can trigger serious events such as hepatic dysfunction [5]. Thus, evaluation of hepatic fat deposition is one of the most important tasks in diagnostic radiology [6-9].

Liver biopsy is known to be the most accurate method for diagnosing fatty liver [10-12]. However, it can only be repeated a limited number of times in a short period and is associated with complications such as infection [13]. Computed tomography (CT) scan has been successfully used to evaluate intra-abdominal

This research was supported by Basic Science Research Program through the National Research Foundation of Korea (NRF) funded by the Ministry of Science, ICT & Future Planning (Grant no. 2021R1F1A1056078 and 2018R1D1A1A02085800)
Corresponding author: Seung-Man Yu, Department of Radiological Science, Jeonju University, 303, Cheonjam-ro, Wansan-gu, Jeonju-si, Jeollabuk-do, 55069, Republic of Korea / Tel:+2-63-220-2382 / E-mail: ysm9993@jj.ac.kr
Received 10 August 2021; Revised 24 August 2021; Accepted 25 August 2021

fat within a short test period [14-16]. However, the quantification of fat deposition inside tissues is virtually impossible and test reproducibility is also limited due to radiation exposure [17]. Quantification of intra-hepatic fat using an ultrasonic test without the risk of exposure to ionized radiation is also difficult, and the inter-observer variations limit the collection of objective data. Even if the experimental method is accurate, it is impossible to observe changes in fatty acid composition of the liver. Magnetic resonance spectroscopy (MRS) can be used to accurately quantify fat composition while overcoming these limitations. MRS can not only analyze the molecular structure using the processed frequency changes caused by differences in physicochemical environment such as ^{1}H, ^{13}C, and ^{31}P protons, but also estimate the concentration of quantified metabolites. In particular, the ^{1}H-MRS lipid analysis can be used to express the respective concentrations: 0.90ppm(methyl), 1.30ppm (methylene), 1.59ppm(methylene proton β to COO), 2.03ppm(methylene protons α to C=C), 2.25ppm(methylene proton α to COO), 2.77ppm(diallylic methylene protons), and 5.31ppm(methane protons). Changes in individual lipid proton(LP) concentration have been used as a basis to diagnose differential and pathological progression of liver fibrosis and steatosis. In addition, the total lipid(TL), total saturated fatty acids(TSFA), total unsaturated fatty acids(TUSFA), total unsaturated bonds(TUSB), and poly unsaturated bonds(PUSB) can be calculated using the concentration ratio of LP[18]. A study using this method to investigate changes in the concentration of specific fatty acids in a rat liver fibrosis model was also conducted, suggesting that different types of fatty acid are deposited in the liver parenchyma depending on the mechanism of liver disease induction. However, few studies investigated the changes in LP composition according to the differences in the pathogenesis of fatty liver.

In order to better represent each of these LP changes, a more precise MRS acquisition technique is essential. A high magnetic field MRI/S scanner provides better resolution and signal-to-noise (SNR). In addition, resolving the problem of J coupling to minimize the influence of adjacent LPs is also one of the important issues to be considered in the data acquisition process. Despite the advantages of these ultra-high field MRI devices, 1.5T and 3T MRI/S scanners are mainly used in humans due to MR safety such as SAR. MRS data acquisition for liver study mainly used STEAM and PRESS pulse sequences. The STEM pulse sequence facilitated more accurate LP quantification because it is less influenced by J coupling. Because of data acquisition with a low SNR value, a high average number increase the probability of test failure in the case of organs moving with the liver. In the case of PRESS, the SNR is two- to three-fold higher than STEM, which reduces the scan time. However, studies disputing the reliability of each quantified LP data have been preceded by the impact on J coupling [19, 20]. Therefore, it is feasible to apply the PRESS pulse sequence to liver MRS data. We determined LP concentration difference degree by applying STEAM and PRESS pulse sequences via phantom experiments. Thus, LP concentration of liver was evaluated in 3T PRESS pulse sequence based on comparison of LP concentrations determined by PRESS and STEAM pulse sequences. In addition, we evaluated the changes in LP in animal models to determine the differences in the mechanism of liver disease such as toxicology, obesity and alcoholic fatty liver, starting with obese fatty liver.

In this study, we investigated the LP concentration according to the differences in induced mechanism of various fatty livers. We suggest using it as basic data for the development of treatment and diagnosis of fatty liver in the future. It is the first study of its kind to observe the changes in LP, which represent hepatic lipids before and after induction of obese fatty liver.

II. Material and Methods

1. Phantom study to identify differences between STEAM and PRESS Pulse sequences of LP concentration

We designed a phantom containing 43 mM sodium

Table 1. The 9.4T in-vitro phantom MRS experiment PRESS and STEAM pulse sequence parameters

TR (time to repeat)	TE (time of echo)	number of average / water un-suppression	acquisition data point	acquisition bandwidth	mixing time
5000msec	20msec	128 / 16	2048	2048	
5000msec	20msec	128 / 16	2048	2048	10msec

dodecyl sulfate (surfactant), 43 mM sodium chloride, 3.75 mM sodium azide, 0.3 mM gadobenate dimeglumine, and 20% soybean oil in deionized water. Soil bean oil has an appropriate LP profile compared with other edible oils. A 9.4 T MRI animal scanner (Biospec 94/20 USR, Bruker Biospin GmbH, Ettlingen, Germany) with a four-channel receive-only array animal coil was used for lipid phantom data acquisition. The T2-weighted image was obtained first in order to perform voxel localization of MRS acquisition, and MRS data were obtained as shown in Table 1 using PRESS and STEAM pulse sequences. The voxel located in the center of the lipid phantom was obtained, and data were acquired with water both for suppressed and unsuppressed signal to calculate water scaling LP concentration value.

2. Animal model of fatty liver

This experiment was conducted in accordance with the "Guidelines for the Management and Use of Laboratory Animals" of the National Institute of Health, which provides health guidance for animal experimental research, and followed a protocol approved by the Animal Experiment Committee of Korea Basic Science Institute (KBSI-AEC 1305). Ten male Sprague-Dawley rats weighing about 100 to 150g were housed in an aseptically isolated space at room temperature (20.5 ± 2°C) and constant relative humidity of 45 ~ 60%. In door illumination was turned on/off during a 12-hour cycle (from 9:00 AM to 9:00 PM). High-fat diet and water were arbitrarily supplied in order to adjust the rats to the environment during the entire experimental period. High-fat diet 60% (D12492, Research Diets, New Brunswick, NJ, 60% fat, 20% protein, and 20% carbohydrate) was used to feed Sprague-Dawley rats to induce fatty liver. Baseline MRI and MRS data (control group) were obtained prior to the introduction of the high-fat diet. Data acquisition experiments were performed after eight weeks using a procedure identical to that of the baseline, since the study results of Takahashi et al. showed that the fatty liver developed after eight weeks [21].

3. Phantom study to identify differences between STEAM and PRESS Pulse sequences of LP concentration

The rat liver was subjected to in vivo MRI/spectroscopy using a 3.0 Tesla MRI (Achiva Tx 3.0 T; Philips Medical Systems, Netherlands) with a four-channel receive-only animal coil (CG-MUC18-H300-AP, Shanghai Chenguang Medical Technologies Co., Ltd., China). In order to obtain the MRI/S data of the experimental animals, respiratory anesthesia was administered by nose cone, maintaining the isoflurane/air to 1.0 to 1.5% and controlling the respiratory cycle frequency to 15-30 times per minute via respiration gating. The volume of interest (VOI) to acquire the MRS data in the liver parenchyma was set to the T2-weighted fast spin echo imaging (T2WI). T2WI was performed in the whole liver parenchyma in the three directional sections of trans axial (FOV 60 mm×60 mm, slice thickness = 1.5 mm), coronal (FOV 60 mm×60 mm, slice thickness = 1.5 mm), and sagittal plan (FOV 60 mm×60 mm, slice thickness = 1.5 mm). The parameters were set as follows: a repetition time = 3000 msec, echo time = 104 msec, matrix = 256×256, section thickness = 1 mm, and number of repetitions = 1. In order to obtain the ^{1}H-MRS data, a point-resolved spectroscopy(PRESS) sequence was used along with TR=1,500msec, TE=35msec, and NEX=64. A8×8×8 mm^3 voxel was also set. The VOI was located near the right side of the liver showing homogeneous signal intensity of liver parenchyma, avoiding large blood vessels, as shown in Fig. 1. For data acquisition, the width of the lipid peak was set

to 4-6Hz using the method of iterative VOI shim, and the method of variable pulse power and optimized relaxation delays(VAPOR) was used for water signal suppression prior to data acquisition.

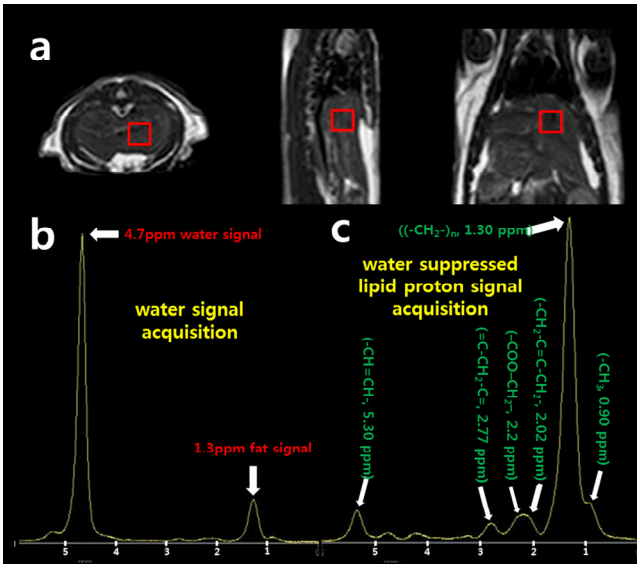

Fig. 1. Typical ^{1}H magnetic resonance spectroscopy of fatty liver rat model with voxel($0.8\times0.8\times0.8cm^3$) placement shown in the T2-weighed axial, sagittal, and coronal turbo spin images. As shown in (a), the signal intensity in the parenchyma was constant and concentrated on the right side of the liver avoiding major vessel, (b) six lipid protons of the parenchyma in the liver: (- CH_3;0.90ppm); methylene proton((- CH_2 -)n, 1.30 ppm); allylic protons (- CH_2 - C=C - CH_2 - , 2.02 ppm); α-methylene protons to carboxyl(-COO-CH_2-,2.2ppm); diallylic protons(=C - CH_2 - C=, 2.77 ppm); and methane protons (- CH=CH - ; 5.30 ppm).

4. MRS and statistical analysis

After the 9.4T lipid phantom and 3T in vivo rat liver MRS experiment were completed, the MRS raw data of all lipid proton metabolites were analyzed by LCModel software (version 6.31H, Stephen W. Provencher). The lipid proton metabolite concentration in the liver of the subject animals was calculated using LCModel, and the analysis was carried out according to the guidelines of LCModel & LCMgui User's manual. Data points of less than 10% of the CramerRao (standard deviation of SNR) value, representing the confidence level of the quantified concentration, were excluded from the analysis in this study. As shown in Fig. 1 (c), quantitative analysis of the hepatic lipid was calculated according to the fat percentage of water scaled six lipid protons.

5. Quantification of lipid protons

The MRS data of the liver parenchyma were compared with those of methyl protons ($-CH_3$;0.90ppm), methylene proton(($-CH_2-$)n;1.30ppm), allylic protons($-CH_2-C=C-CH_2-$;2.02ppm), α -methylene protons to carboxyl (-COO-CH_2-;2.25ppm), diallylic protons(=C-CH_2-C=; 2.77ppm), and methane protons($-CH=CH-$;5.31ppm).

6. Histology

The histological evaluation was conducted to confirm the pathology of hepatic fat deposition after all the experiments were completed. Liver tissues derived from 8 fatty liver animal models were extracted and fixed with 4% formalin, embedded in paraffin, sectioned, and examined under light microscopy after standard hematoxylin-eosin staining.

Ⅲ. Results

The water signal intensity was 423.66 and 823.35 on STEAM and PRESS pulse sequences, respectively, in the phantom study. Each LP concentration was quantified with water normalization. Each LP concentration value on STEAM was higher than in PRESS pulse sequence as shown in Table 2, and the total lipid percentage was 21.25% and 19.20% with STEAM and PRESS pulse sequences, respectively.

The two rats were killed during the baseline testing phase of the in vivo rat fatty liver. Eight rats completed fatty liver modeling and MRS data acquisition finally. We confirmed adequate fat deposition in liver biopsies after all the experiments involving rat liver tissue (Fig. 2). In the rat baseline study before fatty liver development, data with 10% or more of CramerRao consisted of one of the methane protons and another one in the allylic protons. In the MRS performed eight weeks after administering the high-fat diet, no data

Table 2. Results of in vitro experiment of each lipid proton concentration/water ratio value based on PRESS and STEAM pulse sequences.

	Water (primary signal intensity)	0.90 ppm	1.30 ppm	1.59 ppm	2.03 ppm	2.25 ppm	2.77 ppm	5.31 ppm
PRESS	1 (823.35)	0.0217	0.1180	0.0053	0.0175	0.0099	0.0075	0.0121
STEAM	1 (423.66)	0.0241	0.1230	0.0100	0.0206	0.0110	0.0076	0.1620

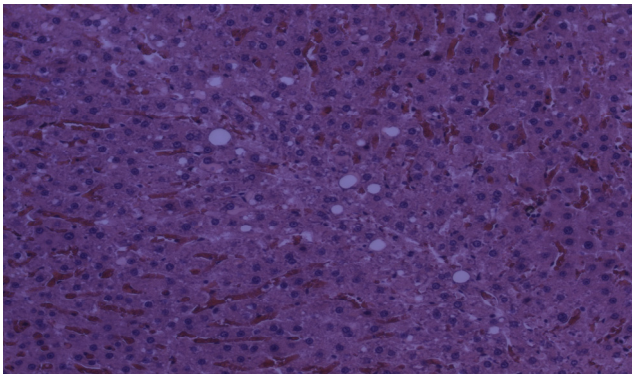

Fig. 2. Rat model of fatty liver tissue induced with H&E stain

representing more than 10% of CramerRao appeared, and the fatty liver data of the eight rats prior to and after exposure to high-fat diet were analyzed for the corresponding comparison of average values.

The average concentration of methylene proton/water proton was found to be 0.038 (3.8%). The concentration of the other LP was very small with insignificant variation. Following the development of fatty liver induced by high-fat diet, the LP increased as a whole, although the ratio of the LP uptake varied (Table 3).

Raw data of fatty liver MRS induced by high-fat diet showed the highest methylene proton/water proton at 1.3 ppm (Table 4), similar to the baseline results. Since the experimental results did not satisfy normality according to the Kolmogorov-Smirnov test, the corresponding t-test was performed as a nonparametric statistical method. Fig. 3 shows the ratio of each LP to total LP prior to and after the development of fatty liver. It was difficult to evaluate the significance difference of each LP concentration

Table 3. The baseline values and results of fatty liver in MRS analysis were obtained before induction of the fatty liver, and the obtained data were scaled according to the concentration of water proton in the liver.

	Case	0.90 ppm	1.30 ppm	2.02 ppm	2.3 ppm	2.77 ppm	5.30 ppm	Sum of fat percentage
control group	1	0.004	0.018	0.002	0.002	0.002	0.008	3.61%
	2	0.002	0.057	0.007	0.010	0.007	0.002	8.49%
	3	0.007	0.032	0.004	0.003	0.005	0.000	5.20%
	4	0.010	0.030	0.006	0.004	0.007	0.004	5.95%
	5	0.005	0.031	0.006	0.011	0.013	0.003	6.88%
	6	0.005	0.052	0.002	0.005	0.002	0.009	7.39%
	7	0.006	0.048	0.004	0.003	0.003	0.005	6.94%
	8	0.006	0.040	0.002	0.003	0.002	0.003	5.57%
	average	0.006	0.038	0.004	0.005	0.005	0.004	6.25%
experimental group	1	0.012	0.148	0.007	0.015	0.010	0.022	21.51%
	2	0.010	0.165	0.014	0.026	0.018	0.013	24.60%
	3	0.021	0.208	0.018	0.024	0.020	0.020	31.18%
	4	0.015	0.201	0.006	0.018	0.009	0.031	28.10%
	5	0.025	0.362	0.013	0.027	0.014	0.046	48.66%
	6	0.024	0.237	0.011	0.022	0.012	0.028	33.48%
	7	0.037	0.387	0.013	0.031	0.017	0.041	52.64%
	8	0.038	0.231	0.002	0.016	0.012	0.003	30.13%
	average	0.023	0.242	0.011	0.022	0.014	0.026	33.79%

Table 4. The results of each lipid proton concentration ratio with total lipid proton

	Case	0.90 ppm	1.30 ppm	2.02 ppm	2.30 ppm	2.77 ppm	5.30 ppm
control group	case 1	0.120	0.490	0.058	0.056	0.043	0.232
	case 2	0.028	0.667	0.088	0.117	0.079	0.021
	case 3	0.142	0.623	0.084	0.065	0.087	0.000
	case 4	0.168	0.498	0.096	0.066	0.111	0.061
	case 5	0.071	0.454	0.090	0.160	0.189	0.036
	case 6	0.072	0.701	0.023	0.061	0.022	0.120
	case 7	0.082	0.687	0.063	0.048	0.041	0.078
	case 8	0.108	0.725	0.037	0.049	0.032	0.050
	average	9.896%	60.563%	6.745%	7.773%	7.540%	7.484%
experimental group	case 1	0.055	0.688	0.035	0.072	0.047	0.104
	case 2	0.041	0.671	0.058	0.104	0.072	0.055
	case 3	0.068	0.667	0.057	0.078	0.064	0.065
	case 4	0.053	0.715	0.023	0.063	0.034	0.112
	case 5	0.051	0.744	0.027	0.056	0.029	0.094
	case 6	0.072	0.708	0.033	0.067	0.037	0.084
	case 7	0.071	0.735	0.025	0.058	0.033	0.078
	case 8	0.127	0.767	0.007	0.052	0.038	0.009
	average	6.722%	71.185%	3.291%	6.868%	4.428%	7.507%

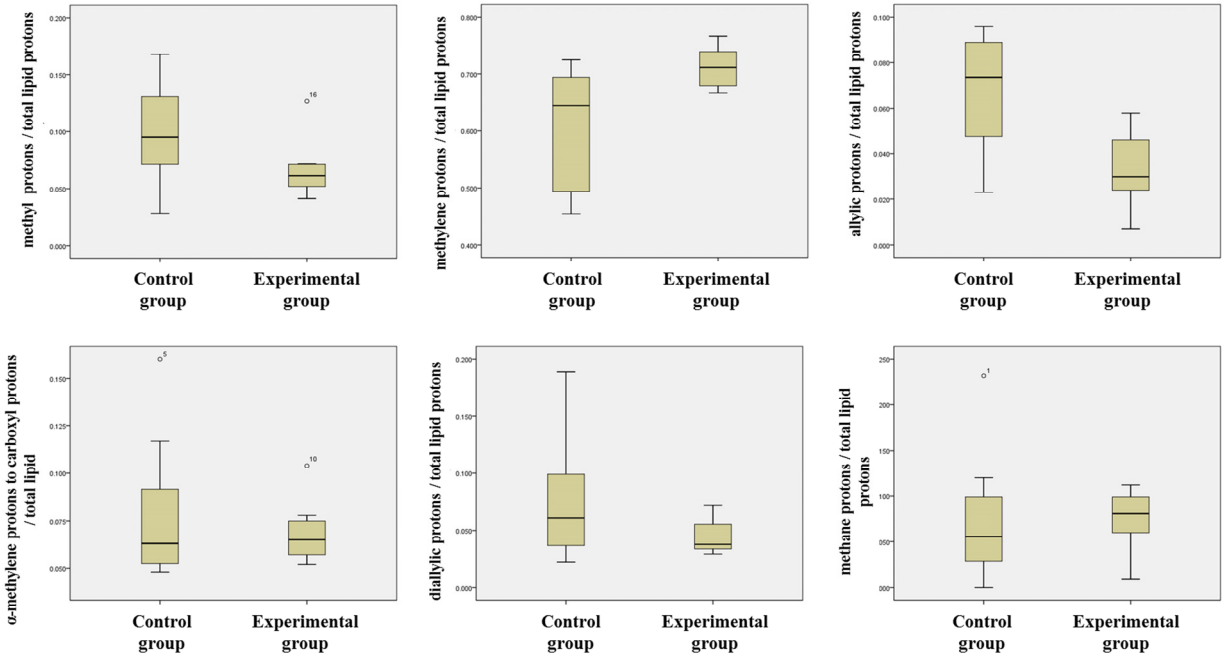

Fig. 3. The ratio of each lipid proton to the total lipid proton prior to and after the induction of fatty liver. For inducing fatty liver, the concentration ratio of the methylene proton largely increased and contributed to the total fat deposition, while the concentration ratios of the methyl protons and allylic proton were relatively low.

as only 8 rat models were compared with baseline data. However, the concentration of methylene proton (1.3 ppm) was higher in the obese fatty liver group. The Spearman test correlating the fat percentage, which is the sum of the total water scaling LP concentrations, and each LP, is shown in Fig. 4.

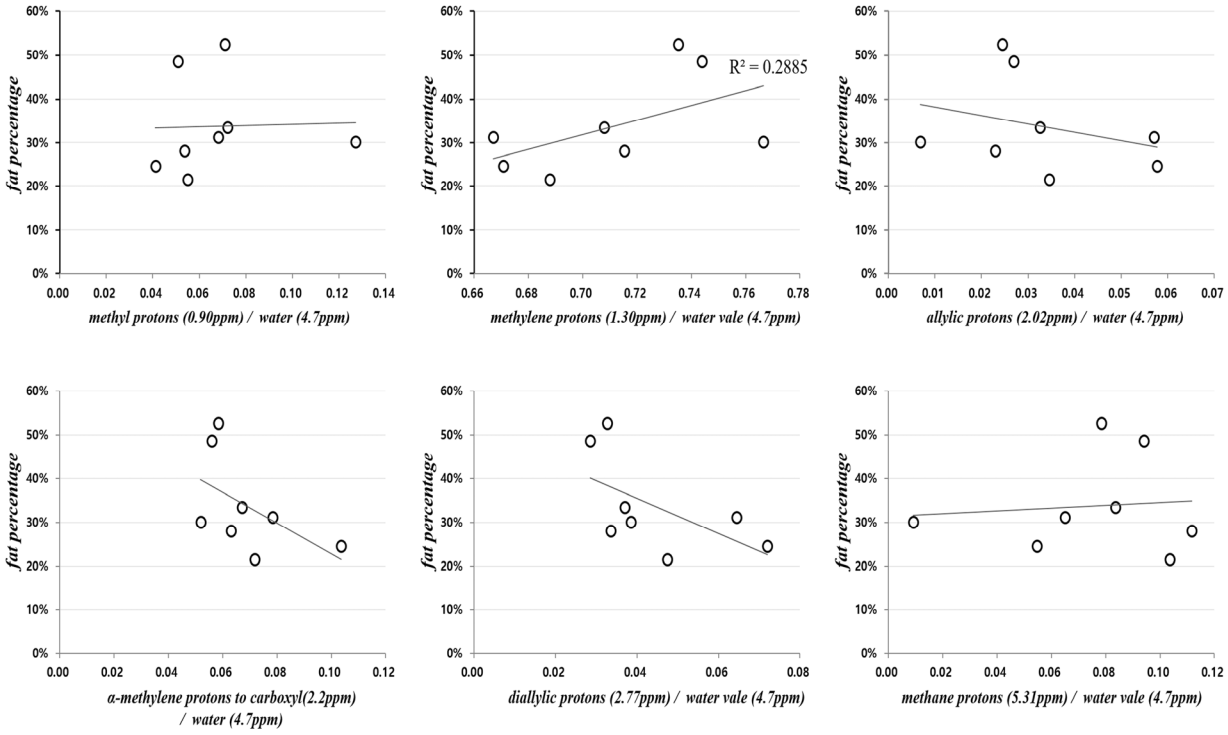

Fig. 4. Correlation of the concentration of each lipid proton in accordance with fat deposition in an animal liver model. During the analysis of the LP and fat percentages of the fatty liver induced, the positive correlation of the methylene protons was the highest, and the increased methylene concentration was considered as the main factor for fat deposition.

The correlation between the fat percentage and each LP, revealed that the methylene protons at 1.3 ppm showed the highest positive correlation. The α −methylene protons to carboxyl(−COO−CH_2−;2.2ppm) and diallylic protons(=C−CH_2−C=;2.77ppm) showed negative correlation with fat percentage.

Ⅳ. Discussion

In this study, precise 20% lipid−water phantom experiments were performed to characterize the respective LP concentrations in liver MRS of PRESS and STEAM. In addition, this study was designed to observe the changes in LPs of fatty livers of obese rats via direct 3T MRI scanner PRESS pulse sequence, which is mainly used in humans. Several studies are currently investigating fatty liver; however, the pathological characteristics of fatty liver and the study of LP changes in fatty liver based on disease mechanism have yet to be studied. This study provides diagnostic information based on the differences in the mechanism of fatty liver development. This study identified the characteristics of fatty liver caused by obesity in particular. In addition, we are currently investigating various mechanisms of fatty liver diseases in addition to obese fatty liver to characterize the pathological changes based on LP concentration. MRS is a valuable tool for the study of factors underlying therapeutic effects, as well as quantitative analysis of metabolites in living organisms and monitoring of disease progression [22−27]. In particular, MRS enables accurate analysis of fatty liver via expression of the fat content as a percentage, unlike biopsy [28]. In previous studies, however, the hepatic fat content was scaled with the water signal ratio only at an LP concentration of 1.3 ppm [29−31], and several trials expressed various concentrations of LP [32−34]. In this study, the changes in each LP concentration were investigated when fat deposition occurred in obese fatty liver.

The 3T MRI device used for in vivo rat liver

experiments provides the highest magnetic field for practical application in humans [35]. Although 7T human MRI scanner has recently been used, it is not generally applicable to the abdomen. The PRESS pulse sequences are commonly used for the evaluation of the degree of hepatic fat deposition. The STEAM pulse sequence provides accurate quantification of each LP concentration with less J coupling effect. Despite these benefits, liver MRS with STEAM is associated with a high possibility of failure due to the relatively long data acquisition time and respiratory effects. For this reason, the use of PRESS pulse sequences with high SNR not only increases the successful outcomes of hepatic study but is also frequently used.

Many studies have been conducted to determine accurate fat composition using STEAM and PRESS in fatty liver. Gavin et al evaluated J coupling effects in both STEAM and PRESS pulse sequences and applied T2 correction via multi TE. LP concentration with T2 correction yields objective information. Song et al developed an accurate rat model of fatty liver LP concentration using pulse sequences of STEAM and PRESS with T2 correction[20]. However, the T2 was calculated as the signal intensity averaged for each TE in this study. Therefore, it is difficult to show that the T2 value was corrected absolutely because of the differences in liver LP signal intensity in each rat model. However, our study did not perform T2 correction strictly, because we never intended to provide accurate fat percentage but to observe the changes in specific LP concentration during fatty liver formation. Therefore, we performed this study only by verifying the accuracy of two pulse sequences using precise percentages of lipid phantom based on PRESS and STEAM pulse sequences with 9.4T. Thus, we determined that if we accurately measured the total fat percentage of the lipid phantom using in vitro phantom experiments, changes in LP concentration could be easily observed in vivo (Fig. 5).

The pulse sequence accuracy of the 20% lipid phantom test was underestimated about 0.8% in PRESS and overestimated 1.25% in STEAM [36]. The reason for the slight variation in total lipid percentage is that trace water evaporates because the buffer solution was heated to fix the lipid-water phantom with agarose gel. Thus, the STEAM, which overestimated total lipid percentage can be used to measure each LP concentration more accurately. As shown in Table 2, all LP/TLP of PRESS data were lower than STEAM. In addition, in our observational evaluation of changes in LP according to fatty liver induction, all differences in LP concentration between the two pulse sequences were less than 0.5%. We concluded that no error occurred even if we observed each LP change using 3T PRESS. Therefore, we conducted the in vivo rat experiment using 3T PRESS pule sequence before conducting human experiments.

As shown in Fig. 3, the concentration of methylene proton (1.3 ppm) was the highest during the induction of obese fatty liver, implying that total saturated fatty acid (TSFA), expressed as 1.3/0.9 ppm LP concentration, mainly leads to intra hepatic deposition. The total lipid percentage ratio of methyl protons is lower, which supports this interpretation as shown in Fig. 4.

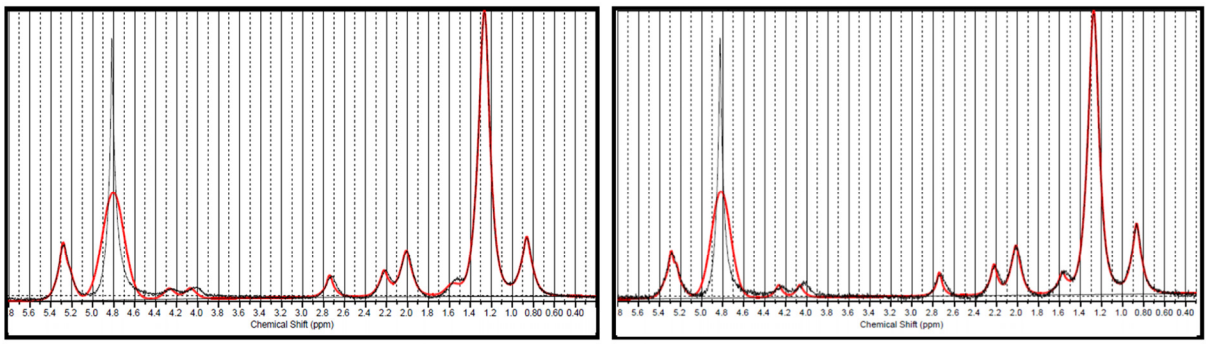

Fig. 5. The results of LCmodel MRS analysis with 9.4T in vitro phantom PRESS and STEAM pulse sequences

As shown in Fig. 3 also the concentrations of α −methylene protons to carboxyl (−COO−CH_2−;2.2ppm) and diallylic protons(=C−CH_2−C=;2.77ppm) were significantly low. No positive correlation existed between LP concentration and fat percentage suggesting that methylene protons are deposited higher when obese fat is deposited intra hepatically. However, the proportion of allylic protons (−CH_2−C=C−CH_2−;2.02ppm) in the total fat percentage was lower. The allylic protons represent TUSFA. We found that obese fatty liver resulted in fat deposition with a high content of saturated fatty acids but a low content of unsaturated fatty acids.

Our study has a few limitations. First, we used 9.4T for the PRESS and STEAM pulse sequences, but did not compare both pulse sequences at 3T. If MRS data analysis of 3.0T PRESS was performed with the same phantom to confirm the identity with LP composition of 9.4T PRESS, more reliable in vivo 3T results may be obtained. Second, our pilot study was carried out with 10 animal models. In particular, two animal models died during the experiment, and 8 animal models were used finally. In order to obtain more objective results, additional experiments involving a higher number of animal models are needed. We are conducting experiments with a greater number of experimental animals to characterize the differences in LP concentration according to the differences in fatty liver−induced mechanism. In addition, this study confirmed the possibility of obtaining meaningful results as the final goal. Therefore, our research team is developing animal models of fatty liver based on five pathological differences.

Ⅴ. Conclusion

In conclusion, we observed changes of each LP using the MRS to analyze fat in the liver parenchyma of induced obese fatty liver. In particular, the 1.3 ppm concentration of methylene proton was associated with the highest increase in fat deposition, and decreased diallylic proton levels.

REFERENCES

[1] Adams LA, Lymp JF, St Sauver J, Sanderson SO, Lindor KD, Feldstein A, et al. The natural history of nonalcoholic fatty liver disease: A population−based cohort study. Gastroenterology. 2005;129(1):113−21.

[2] Lieber CS. Pathogenesis and treatment of alcoholic liver disease: Progress over the last 50 years. Rocz Akad Med Bialymst. 2005;50:7−20.

[3] Marengo A, Jouness RI, Bugianesi E. Progression and natural history of nonalcoholic fatty liver disease in adults. Clin Liver Dis. 2016;20(2):313−24.

[4] Sakamoto M. [1. Clinincal diagnosis and medical care of liver disease, present situation and progress]. Nihon Hoshasen Gijutsu Gakkai Zasshi. 2015;71(12):1265−74.

[5] Han S, Ko JS, Kwon G, Park C, Lee S, Kim J, et al. Effect of pure microsteatosis on transplant outcomes after living donor liver transplantation: A matched case−control study. Liver Transpl. 2014;20(4):473−82.

[6] Kang BK, Yu ES, Lee SS, Lee Y, Kim N, Sirlin CB, et al. Hepatic fat quantification: A prospective comparison of magnetic resonance spectroscopy and analysis methods for chemical−shift gradient echo magnetic resonance imaging with histologic assessment as the reference standard. Invest Radiol. 2012;47(6):368−75.

[7] Kramer H, Pickhardt PJ, Kliewer MA, Hernando D, Chen GH, Zagzebski JA, et al. Accuracy of Liver Fat Quantification With Advanced CT, MRI, and Ultrasound Techniques: Prospective Comparison with MR Spectroscopy. AJR Am J Roentgenol. 2017;208(1):92−100.

[8] Wells SA. Quantification of hepatic fat and iron with magnetic resonance imaging. Magn Reson Imaging Clin N Am. 2014;22(3):397−416.

[9] Wierzbicki AS, Oben J. Nonalcoholic fatty liver disease and lipids. Curr Opin Lipidol. 2012;23(4):345−52.

[10] Hatta T, Fujinaga Y, Kadoya M, Ueda H, Murayama H, Kurozumi M, et al. Accurate and simple method

for quantification of hepatic fat content using magnetic resonance imaging: A prospective study in biopsy-proven nonalcoholic fatty liver disease. J Gastroenterol. 2010;45(12):1263-71.

[11] Malik R, Chang M, Bhaskar K, Nasser I, Curry M, Schuppan D, et al. The clinical utility of biomarkers and the nonalcoholic steatohepatitis CRN liver biopsy scoring system in patients with nonalcoholic fatty liver disease. J Gastroenterol Hepatol. 2009;24(4):564-8.

[12] Adams LA, Angulo P. Role of liver biopsy and serum markers of liver fibrosis in non-alcoholic fatty liver disease. Clin Liver Dis. 2007;11(1):25-35.

[13] Gavril RS, Mihalache L, Arhire L, Grosu C, Gherasim A, Nita O, et al. Is liver biopsy necessary in patients with nonalcoholic fatty liver disease? Rev Med Chir Soc Med Nat Iasi. 2016;120(3):503-7.

[14] Dang J, Xu Y, Wei Y. [Quantitative diagnosis of fatty liver using mask cover of CT image]. Sichuan Da Xue Xue Bao Yi Xue Ban. 2003;34(1):158-9.

[15] Wang B, Gao Z, Zou Q, Li L. Quantitative diagnosis of fatty liver with dual-energy CT: An experimental study in rabbits. Acta Radiol. 2003;44(1):92-7.

[16] Mendler MH, Bouillet P, Le Sidaner A, Lavoine E, Labrousse F, Sautereau D, et al. Dual-energy CT in the diagnosis and quantification of fatty liver: Limited clinical value in comparison to ultrasound scan and single-energy CT, with special reference to iron overload. J Hepatol. 1998;28(5):785-94.

[17] Cutillo DP, Swayne LC, Fasciano MG, Schwartz JR. Absence of fatty replacement in radiation damaged liver: CT demonstration. J Comput Assist Tomogr. 1989;13(2):259-61.

[18] Ren J, Dimitrov I, Sherry AD, Malloy CR. Composition of adipose tissue and marrow fat in humans by 1H NMR at 7 Tesla. J Lipid Res. 2008;49(9):2055-62.

[19] Hamilton G, Middleton MS, Bydder M, Yokoo T, Schwimmer JB, Kono Y, et al. Effect of PRESS and STEAM sequences on magnetic resonance spectroscopic liver fat quantification. J Magn Reson Imaging. 2009;30(1):145-52.

[20] Song KH, Lee MY, Yoo CH, Lim SI, Choe BY. Improved quantitative fatty acid values with correction of T2 relaxation time in terminal methyl group: In vivo proton magnetic resonance spectroscopy at ultra high field in hepatic steatosis. Chem Phys Lipids. 2018;212:35-43.

[21] Takahashi Y, Soejima Y, Fukusato T. Animal models of nonalcoholic fatty liver disease/nonalcoholic steatohepatitis. World J Gastroenterol. 2012;18(19):2300-8.

[22] Fischbach F, Thormann M, Ricke J. [(1)H magnetic resonance spectroscopy (MRS) of the liver and hepatic malignant tumors at 3.0 Tesla]. Radiologe. 2004;44(12):1192-6.

[23] Fonvig CE, Chabanova E, Andersson EA, Ohrt JD, Pedersen O, Hansen T, et al. ^{1}H-MRS Measured Ectopic Fat in Liver and Muscle in Danish Lean and Obese Children and Adolescents. PLoS One. 2015;10(8):e0135018.

[24] Lee Y, Jee HJ, Noh H, Kang GH, Park J, Cho J, et al. In vivo (1)H-MRS hepatic lipid profiling in nonalcoholic fatty liver disease: An animal study at 9.4 T. Magn Reson Med. 2013;70(3):620-9.

[25] Moreno A, Lopez LA, Fabra A, Arus C. ^{1}H MRS markers of tumour growth in intrasplenic tumours and liver metastasis induced by injection of HT-29 cells in nude mice spleen. NMR Biomed. 1998;11(3):93-106.

[26] Wang D, Li Y. ^{1}H magnetic resonance spectroscopy predicts hepatocellular carcinoma in a subset of patients with liver cirrhosis: A randomized trial. Medicine (Baltimore). 2015;94(27):e1066.

[27] Yu SM, Ki SH, Baek HM. Nonalcoholic fatty liver disease: Correlation of the liver parenchyma fatty acid with intravoxel incoherent motion MR imaging-an experimental study in a rat model. PLoS One. 2015;10(10):e0139874.

[28] Dillman JR, Trout AT, Costello EN, Serai SD, Bramlage KS, Kohli R, et al. Quantitative liver MRI-biopsy correlation in pediatric and young adult patients with nonalcoholic fatty liver disease: Can one be used to predict the other? AJR Am J Roentgenol. 2018;210(1):166-74.

[29] Dixon WT. Simple proton spectroscopic imaging. Radiology. 1984;153(1):189-94.

[30] Lee SS, Lee Y, Kim N, Kim SW, Byun JH, Park SH, et al. Hepatic fat quantification using chemical shift MR imaging and MR spectroscopy in the presence of hepatic iron deposition: Validation in phantoms and in patients with chronic liver disease. J Magn Reson Imaging. 2011;33(6):1390-8.

[31] Reeder SB, Bice EK, Yu H, Hernando D, Pineda AR. On the performance of T_2^* correction methods for quantification of hepatic fat content. Magn Reson Med. 2012;67(2):389-404.

[32] Agten CA, Rosskopf AB, Gerber C, Pfirrmann CW. Quantification of early fatty infiltration of the rotator cuff muscles: Comparison of multi-echo Dixon with single-voxel MR spectroscopy. Eur Radiol. 2016;26(10):3719-27.

[33] Yoo YH, Kim HS, Lee YH, Yoon CS, Paek MY, Yoo H, et al. Comparison of Multi-echo dixon methods with volume interpolated breath-hold gradient echo magnetic resonance imaging in fat-signal fraction quantification of paravertebral muscle. Korean J Radiol. 2015;16(5):1086-95.

[34] Ishizaka K, Oyama N, Mito S, Sugimori H, Nakanishi M, Okuaki T, et al. Comparison of ^{1}H MR spectroscopy, 3-point DIXON, and multi-echo gradient echo for measuring hepatic fat fraction. Magn Reson Med Sci. 2011;10(1):41-8.

[35] Min JW, Jeong HW, Han JH, Lee SN, Han SY, Kim KE, et al. Study on the resolution characteristics by using magnetic resonance imaging 3.0T. Journal of Radiological Science and Technology. 2020;43(4):251-7.

[36] Yun SJ, Lim JS, The analysis of brain tumor's grades using magnetic resonance spectroscopy. Journal of Radiological Science and Technology. 2008;31(4):355-65.

구분	성명	소속	직위
제1저자	김상혁	전주대학교 방사선학과, 원광대병원 영상의학과	석사대학원생/방사선사
교신저자	유승만	전주대학교 방사선학과	조교수